Combining bulk sediment OSL and meteoric ^{10}Be fingerprinting techniques to identify gully initiation sites and erosion depths

E. W. Portenga[1,2*], P. Bishop[1], D. H. Rood[3,4], and P. R. Bierman[5]

[1] School of Geographical and Earth Sciences, University of Glasgow, Glasgow, G12 8QQ, UK.

[2] Department of Environmental Sciences, Macquarie University, North Ryde, NSW 2109, Australia.

[3] AMS Laboratory, Scottish Universities Environmental Research Centre, University of Glasgow, East Kilbride G75 0QF, UK.

[4] Department of Earth Sciences and Engineering, Imperial College London, South Kensington Campus, London SW7 2AZ, UK.

[5] Geology Department & Rubenstein School of the Environment and Natural Resources, University of Vermont, VT 05405, USA.

Corresponding author: Eric W. Portenga (ewport@umich.edu)

* Now at Department of Earth and Environmental Sciences, University of Michigan, Ann Arbor, MI 48109, USA.

Key Points:

- First combined use of meteoric ^{10}Be and bulk OSL to trace sediment back to its source
- Sediment source location and depth of initial gully incision are both identified
- Gullies eroded initially into livestock-compressed and drought-stressed valley fill, not water-saturated wetlands
- Approach can be used to trace sediment in landscapes worldwide, including those disturbed by human activity

This is the author manuscript accepted for publication and has undergone full peer review but has not been through the copyediting, typesetting, pagination and proofreading process, which may lead to differences between this version and the Version of Record. Please cite this article as doi: 10.1002/2016JF004052

Abstract

Deep erosional gullies dissect landscapes around the world. Existing erosion models focus on predicting where gullies might begin to erode, but identifying where existing gullies were initiated and under what conditions is difficult, especially when historical records are unavailable. Here, we outline a new approach for fingerprinting alluvium and tracing it back to its source by combining bulk sediment optically stimulated luminescence (bulk OSL) and meteoric ^{10}Be ($^{10}Be_m$) measurements made on gully-derived alluvium samples. In doing so, we identify where gully erosion was initiated and infer the conditions under which such erosion occurred. As both $^{10}Be_m$ and bulk OSL data have distinctive depth-profiles in different uneroded and depositional settings, we are able to identify the likely depths in potential source areas of alluvium. We demonstrate our technique at Birchams Creek in the southeastern Australian Tablelands – a well-studied and recent example of gully incision that exemplifies a regional landscape transition from unchannelled swampy meadow wetlands to gully incision and subsequent wetland burial by post-European settlement alluvium. We find that such historic alluvium was derived from shallow erosion of valley fill upstream of former swampy meadows and was deposited down the center of the valley. Incision likely followed catchment deforestation and the introduction of livestock, which overgrazed and congregated in valley bottoms in the early 20th century during a period of drought. As a result, severe gully erosion was likely initiated in localized, compacted, and oversteepened reaches of the valley bottom.

1.0 Introduction

Gullies are deep erosional features incised into landscapes, too large to be easily filled; they can be formed by natural and anthropogenic processes, often involving land-use changes that reduce native vegetation cover [*Cox et al.*, 2010; *Eriksson et al.*, 2006; *Eyles*, 1977b; *Knox*, 2006; *Nyssen et al.*, 2004; *Reusser and Bierman*, 2010; *Stankoviansky*, 2003]. The consequences of gully erosion are two-fold: incision and expansion of gullies in up-catchment landscapes erodes soil [*Perroy et al.*, 2010; *Poesen et al*., 2003; *Reusser and Bierman*, 2010], and deposition of gully-derived sediment fills and buries down-catchment landscapes on both short and long term timescales [*Beach et al.*, 2006; *Coronato and del Valle*, 1993; *Eyles*, 1977b; *Garcia-Rodríguez et al*., 2002; *Luk et al*., 1997; *Nichols et al*., 2014; *Valette-Silver et al*., 1986]. While natural gully incision may be unpreventable [*Cox et al*., 2010; *diCenzo and Luk*, 1997; *Gellis et al.*, 2011; *Luk et al*., 1997], gully incision following changes in human land-use practices is often, in hindsight, preventable [e.g. *Brannstrom and Oliveira*, 2000; *Eyles*, 1977b; *Fuchs et al*., 2004; *Montgomery*, 2007; *Perroy et al.*, 2010; *Reusser and Bierman*, 2010; *Richardson et al*., 2014; *Rosen*, 2008; *Stankoviansky*, 2003; *Turkelboom et al*., 2008; *Valette-Silver et al*., 1986]. Whether initiated by natural or anthropogenic causes, gullies affect landscapes around the world, and understanding the conditions under which they are likely to form is crucial to preparing for and possibly mitigating soil and environmental losses resulting from erosion and sediment deposition.

Topographic threshold models attempt to predict where gully incision might initiate [*Patton and Schumm*, 1975; *Vandaele et al.*, 1996]. Other studies show that gully walls and beds become the source of the majority of sediment produced from gullied landscapes [*Krause et al.*, 2003; *Olley et al.*, 1993]. However, no studies demonstrate, in the absence of recorded observation, procedures for identifying where in a landscape existing gullies were initiated, information that is necessary to understand the causes of gully erosion. In this study, we outline and test one such procedure.

Retrospectively identifying where sediment eroded from gullies originated within a landscape requires a means of monitoring sediment from, or tracing sediment back to, its source. A number of techniques have been used to do this, including radiogenic and cosmogenic isotopes, sediment luminescence, thermochronology, radio tagging, and remote sensing, amongst others [*Bradley and Tucker*, 2012; *D'Haen et al.*, 2012; *Lamarre et al.*, 2005; *Muñoz-Salinas et al.*, 2014; *Nelson et al.*, 2014; *Rengers et al.*, 2016; *Reusser and Bierman*, 2010; *Stock et al.*, 2006; *Wasson et al.*, 2002]. When used alone, these techniques can identify detrital sediment source regions, elevations, or lithologies; however, combining multiple techniques has the potential to expand our understanding of geomorphological processes and landforms. For example, multiple geochronometers have been used to independently date landforms such as fault scarps and alluvial surfaces [*Bierman et al.*, 2014; *Blisniuk et al.*, 2012; *Nissen et al.*, 2009] and to understand regolith production and mixing on hillslopes [*Dosseto et al.*, 2008; *Ma et al.*, 2013; *West et al.*, 2013; *Wilkinson et al.*, 2005]. Some techniques have been combined to quantify and monitor sediment transport through fluvial systems, but the number and variety of examples are fewer [e.g. *Dosseto and Schaller*, 2016; *Wasson et al.*, 2002].

Testing ideas about gully incision into landscapes using different sediment tracing techniques requires preservation of sediment deposits that resulted from gully erosion. To this end, the presence of post-(European) settlement alluvium (PSA) in landscapes around the world makes it an ideal such material. Prior to the European colonial era, PSA was often eroded from gully systems that formed as a result of land-use practices being introduced to a landscape that had been previously uninhabited such as in the Americas, Iceland, Africa, Europe, and Asia [e.g. *Beach et al.*, 2006; *Coltorti et al.*, 2010; *Dugmore et al.*, 2000; *Kidder et al.*, 2012; *Nyssen et al.*, 2014; *Pope and van Andel*, 1984; *Rosen*, 2008]. More commonly known is landscape erosion and PSA deposition across regions that were affected by European and American colonial expansion and industrial intensification in the 17^{th}–19^{th} centuries throughout North America, South Africa, Europe, Oceania, and South America [e.g. *Brannstrom and Oliveira*, 2000; *Damm and Hagedorn*, 2010; *Foulds et al.*, 2013; *Garcia-Rodríguez et al.*, 2002; *Montgomery*, 2007; *Richardson et al.*, 2014; *Portenga et al.*, 2016a, 2016b; *Rustomji and Pietsch*, 2007]. Not only is PSA an ideal material for this study because of its connection to gully erosion, but also its relationship to human land use around the world provides insights into the magnitude of historical and pre-historical human impacts on global landscapes and environments [*Hooke et al.*, 2012; *Montgomery*, 2007; *Toy*, 1982; *Wilkinson and McElroy*, 2007].

In this study, we combine the sediment fingerprinting capabilities of bulk optically stimulated luminescence (bulk OSL) and meteoric cosmogenic ^{10}Be ($^{10}Be_m$) to trace PSA deposited in Birchams Creek, a small catchment in the southeastern Australian Tablelands, back to its source. These two techniques have never been applied together in a geomorphological context and we demonstrate how we are able to infer the most reasonable gully erosion history for Birchams Creek by comparing depth profiles of bulk OSL and $^{10}Be_m$ in PSA and from potential source locations. The widespread use of OSL and $^{10}Be_m$ in geomorphological studies allows our research approach to be adapted elsewhere to form a more complete understanding of how human land use shapes the landscapes in which people live.

2.0 Background

2.1 Field Area

Widespread gully incision and PSA deposition occurred in the Tablelands region of southeastern Australia (Figure 1), where the causes and timing of gullying and the connection between gullying and PSA deposition have been at the center of research efforts for decades [*Crouch*, 1987; *Eyles*, 1977a; *Mould and Fryirs*, 2017; *Muñoz-Salinas et al.*, 2011, 2014; *Neil and Fogarty*, 1991; *Olley et al.*, 1993; *Olley and Wasson*, 2003; *Portenga et al.*, 2016b; *Prosser and Slade*, 1994; *Rustomji and Pietsch*, 2007; *Starr*, 1989; *Wasson et al.*, 1998]. Catchment conditions and land-use practices leading to initial gully incision are often not considered [*Prosser and Slade*, 1994; *Prosser and Winchester*, 1996], though they are generally understood to involve vegetation disturbance along valley sides and bottoms, like those imposed by arid climate conditions or those introduced by European settlers in the 19th and 20th centuries [*Eyles*, 1977a, 1977b; *Portenga et al.*, 2016b; *Prosser*, 1991; *Rustomji and Pietsch*, 2007; *Scott*, 2001; *Starr*, 1989; *Zierholz et al.*, 2001].

This study focuses on Birchams Creek, a 3.8 km^2 headwater tributary of the Yass River about 15 km northeast of Canberra, Australia (Figure 1). Eyles [1977a] studied a chain of ponds in Birchams Creek and its evolution into a continuous gully (Figure 1), a process that occurred regionally soon after European arrival in the early 1800s CE [*Eyles*, 1977b]. The first surveys of the creek in 1880 CE show swampy meadow wetlands and chains of ponds [*Mactaggart et al.*, 2008] within the lower reaches of the creek before trees were ring barked (e.g. girdled) and cleared in the early 20th century; landowners observed a gully present at the mouth of the creek in 1910 CE [*Eyles*, 1977a] (Figure 2a). At present, the upper reaches of Birchams Creek are underlain by light-colored loamy distal hillslope deposits, likely with some alluvial component, weathered from the Adaminaby Group, which underlies the whole catchment; we term these sediments valley fill (VF). The lower reaches of the creek had once been characterized by distinctive clayey, organic-rich swampy meadow (SM) wetlands; SM sediments are now overlain by thick deposits of PSA, which were deposited between 1914–1932 CE following European-introduced land-use changes [*Portenga et al.*, 2016a, 2016b].

At present, the lower 1.4 km of the Birchams Creek is a deep erosional gully, up to ~4 m deep (Figure 2b-e). Progressing headward from the catchment mouth, stratigraphy exposed in the gully walls are firstly dark clay-rich SM sediment overlain by PSA (site PSA-1; Figure 1), then SM sediment not covered by PSA (site SM-1), another sequence of SM overlain by PSA (site PSA-2), and finally VF (site VF-1), which covers the remainder of the upstream valley bottom (Figure 1). PSA at both sites PSA-1 and PSA-2 is incised by the modern gully – an indication that PSA deposition occurred prior to headward migration of the gully observed in 1910 CE. PSA in Birchams Creek is a sandy loam with lenses of gravel exposed stratigraphically above SM in the lower and middle reaches of Birchams Creek (Figure 1) and can be >1 m thick (Figure 3). Though we were unable to map the lateral extent of PSA, it is seen exposed on both sides of gully walls; as elsewhere in the Tablelands, we assume that PSA was deposited across the valley bottoms [*Portenga et al.*, 2016a., 2016b; *Rustomji and Pietsch*, 2007].

Increased overland flow is typically cited as the main triggering mechanism driving gully incision [*Poesen et al*., 2003; *Prosser*, 1991; *Prosser and Abernethy*, 1996], although exactly where within a given drainage overland flow has the greatest effect is uncertain. Field-based flume experiments in the Tablelands have shown that clayey SM sediments resist erosion unless both vegetation is degraded and discharge increased [*Prosser and Slade*, 1994]; moreover, newly-established swampy vegetation in modern gully beds is able to withstand modern floods [*Zierholz et al.*, 2001]. These findings support the notion that wetlands, though water-saturated, are not likely to be the site of initial gully incision. Others have instead suggested that PSA is more likely derived from erosion into previously-deposited VF sediment [*Eyles*, 1977a; *Prosser*, 1990; *Wasson et al.*, 1998]. Whether gullies, now regionally common, were more likely to incise into SM sediment or VF is a focus of this study.

2.2 Gully initiation conceptual models

The majority of sediment transported out of modern gully systems in the Tablelands comes from gully bed and gully bank erosion with minimal sediment being derived from hillslopes [*Neil and Fogarty*, 1991; *Olley et al.*, 1993]. Assuming, then, that all PSA comes from valley bottom erosion, and not from hillslopes, there are two possible PSA erosional histories at Birchams Creek. In the discontinuous gully erosion conceptual model (DGECM), gully initiation occurs at multiple locations: alluvium at PSA-1 being sourced from incision at SM-1 at the same time that alluvium at PSA-2 was sourced from incision at VF-1 (Figure 4a). Alternatively, in the single site erosion conceptual model (SSECM), gully erosion was initiated at VF-1 and supplied alluvium to PSA-1 and PSA-2 (Figure 4b). In the DGECM, eroded sediment is transported along the modern stream channel, which was later incised by headward erosion of the 1910 CE gully. In the SSECM, eroded sediment from VF-1 is deposited along the axis of the valley, after which the 1910 CE gully must have eroded from PSA-1 into SM sediments at SM-1 and then back into alluvium at PSA-2.

3.0 Methods

The uniform bedrock underlying Birchams Creek and its single channel are useful for this study in that measured variations of bulk OSL and $^{10}Be_m$ concentrations of sediment within the catchment should only result from changes affecting erosion and depositional conditions within the catchment. Luminescence accumulation in mineral grains is directly proportional to the rate and duration of the 'dose' of ionizing radiation from the surrounding sediment [*Aitken*, 1998]. Luminescence can be completely removed by sufficient exposure to sunlight during sediment transport – a process called bleaching. However, sediment in fluvial systems is often incompletely bleached [*Jain et al.*, 2004; *Rittenour*, 2008; *Wallinga*, 2002], and inherited luminescence has previously been observed for catchments throughout the Tablelands [*Muñoz-Salinas et al.*, 2011, 2014; *Olley et al.*, 1998; *Portenga et al.*, 2016b]. At Birchams Creek, single-grain quartz OSL equivalent doses for PSA at site PSA-1 are bimodal with a clear upper limit, which has been inferred as inheritance from the source material that was incompletely bleached during sediment transport [*Portenga et al.*, 2016b]. Muñoz-Salinas et al. [2014] reached a similar conclusion, suggesting that the least completely-bleached fraction of fluvial sediment (i.e. that which is emitted during bulk OSL measurement) is inherited from the sediment's parent material, which allows that luminescence to be used to trace sediment through a stream network to the sediment's source. By measuring bulk OSL data in PSA sediment and comparing the results to characteristic bulk OSL profiles of uneroded SM and VF sediments, we are able to infer the geographical source of PSA and the initial incision depth.

$^{10}Be_m$ is produced in the atmosphere through spallogenic interactions between secondary cosmic ray-derived neutrons and O and N target nuclei [*Lal and Peters*, 1967]. $^{10}Be_m$ is delivered via precipitation and dry fallout to the Earth's surface where it is strongly adsorbed to sediment grains and accumulates in soil profiles, forming characteristic depth profiles [*Fifield et al.*, 2010; *Graly et al.*, 2010; *Monaghan et al.*, 1986; *Willenbring and von Blanckenburg*, 2010]. Because $^{10}Be_m$ adheres strongly to sediment grains, it has been used as a sediment tracer in a number of geomorphic settings [*Brown et al.*, 1988; *Helz and Valette-Silver*, 1992; *Reusser and Bierman*, 2010]. Characteristic depth profiles of $^{10}Be_m$ therefore provide a secondary and independent assessment of PSA sediment provenance and initial incision depth.

Sediment samples for both bulk OSL and $^{10}Be_m$ measurements were collected at each of the four sites in Birchams Creek: PSA-1, PSA-2, SM-1, and VF-1 (Figures 1, 2). Bulk OSL samples were measured at 3 cm depth intervals to a depth of ~1 m at all sites and sediment profile descriptions were recorded (Figure 3); deeper sampling at SM-1 continued at 5 cm intervals. $^{10}Be_m$ samples were collected as point samples at 9 cm depth intervals at PSA-1, PSA-2, and VF-1, to depths of 102 cm, 75 cm, and 81 cm, respectively, and at 12 cm depth intervals at SM-1 to a depth of 112 cm.

Samples were measured for bulk OSL using a portable OSL reader [*Sanderson and Murphy*, 2010]. Each polymineral, poly-grain size sample was stimulated by both infrared and blue-light LED sources (60 s, each). Dark counts – photon counts detected in the absence of stimulation – were also measured prior to and after infrared and blue-light stimulation. Photon

counts emitted from bulk OSL sediment following stimulation cycles were summed such that each bulk OSL measurement reflects the total luminescence emitted from all grain-sizes and mineral phases in each bulk sediment sample minus the luminescence measured during dark counts (Figure S1). Bulk sediment OSL samples include a large number of grains, making it possible for a few rare, highly-sensitive (e.g. bright) grains to overwhelm the bulk OSL measurement and produce unusually high bulk OSL measurements [*Rhodes*, 2007]. To counter this possible effect, we smoothed the bulk OSL depth-profiles using a 3-sample moving average (Figure 5a). Bulk OSL data from sample replicates measured from well-bleached SM sediments converge on similar values; bulk OSL data from PSA sediment replicates show variability, however, likely resulting from measuring the luminescence of incompletely bleached samples or from the inclusion of a few bright grains (see Figure 4 in [*Portenga et al.*, 2016a]). Although PSA exhibits more variable luminescence in replicate sampling, the overall depth trends of bulk OSL data through PSA profiles replicate well, even when measurements are made years apart [*Portenga and Bishop*, 2016].

$^{10}Be_m$ was measured on the same samples as were used for bulk OSL analyses. Soil pH for all samples was measured using powdered pH indicators and values range from 5.5–7; thus, we assume that no $^{10}Be_m$ has been remobilized after being adsorbed to sediment. $^{10}Be_m$ samples were processed at the University of Vermont Cosmogenic Nuclide Laboratory where they were milled, and ~0.5 g of powdered sample was mixed with ~0.4 g of ^{9}Be solution (SPEX 1000 ppm). A modification of Stone's [1998] fusion method was used to extract beryllium, which was burned to produce beryllium oxide. Each sample was then mixed with Nb powder at a 1:1 molar ratio before being packed into copper cathodes to be analyzed using accelerator mass spectrometry (AMS) at the Scottish Universities Environmental Research Centre (SUERC) [*Xu et al.*, 2015]. Measured ^{10}Be/^{9}Be ratios were normalized to NIST SRM4325 standard material with a ^{10}Be/^{9}Be ratio of 2.79×10^{-11} and blank-corrected using three process blanks (avg. = $1.71 \pm 0.83 \times 10^{-14}$), from which concentrations of $^{10}Be_m$ are derived; blank corrections were <0.1% of measured ^{10}Be/^{9}Be ratios. AMS measurement uncertainties for $^{10}Be_m$ concentrations are 1σ and average 2% for all samples, and uncertainties in the samples and blanks were propagated in quadrature. $^{10}Be_m$ sample material from SM-1 at a depth of 63 cm was split and each half of the sample was processed, yielding $^{10}Be_m$ concentrations of $18.6 \pm 0.44 \times 10^{8}$ atoms/g and $18.8 \pm 0.34 \times 10^{8}$ atoms/g, a difference of 1.4%. The similarity between these replicate samples demonstrates the reproducibility and consistency of the $^{10}Be_m$ extraction methods used and the $^{10}Be_m$ results presented.

4.0 Results

The SM-PSA transition at PSA-1 and PSA-2 occurs at the depth at which changes in sediment texture and color (Figure 3) and changes in bulk OSL depth trends coincide [*Portenga et al.*, 2016a]. Below the SM-PSA transition, bulk OSL measurements in SM sediment at PSA-1 and PSA-2 systematically decrease up-profile to the SM-PSA transition at 99 and 72 cm, respectively (Figure 5a). The bulk OSL data at depths below the SM-PSA boundary at PSA-1

appear, in the figure, not to increase with depth but this is only because the magnitude of bulk OSL data for these samples is small relative to the bulk OSL maximum values measured in the overlying PSA (Table S1). Luminescence measurements increase above the SM-PSA transition to a maximum 3-sample average value of 3.4×10^6 photon counts at PSA-1 (54 cm) and 2.4×10^6 photon counts at PSA-2 (57 cm). Bulk OSL data from SM-1 are near zero at the valley bottom surface and increase with depth to ~65 cm in the SM exposure (Figure 5a); bulk OSL data at SM-1 exhibit maxima at ~65 cm and ~130 cm. Bulk OSL depth trends at VF-1 show a small bulge in the uppermost 20 cm, beneath which bulk OSL data increase systematically to a depth equal to that of the gully bed (Figure 5a); there is perhaps a third bulk OSL increase at a depth of ~50 cm.

$^{10}Be_m$ measurements are similar throughout PSA profiles and average $8.2 \pm 0.8 \times 10^8$ atoms/g and $8.2 \pm 0.3 \times 10^8$ atoms/g at PSA-1 and PSA-2, respectively (Figure 5b, Table S2). The main difference between the profiles is at a depth of 21 cm at PSA-1 where a horizon of coarse gravel is exposed along with fine sandy clay loam (Figure 3a); no such horizon exists at PSA-2. At $16 \pm 0.3 \times 10^8$ atoms/g, the meteoric ^{10}Be content of this horizon at PSA-1 corresponds to an isolated increase in $^{10}Be_m$ well above the average, likely representing the isotopic content of the finer-grained matrix rather than the gravel. Measurements of $^{10}Be_m$ at SM-1 exhibit an increase in concentration from $8.3 \pm 0.16 \times 10^8$ atoms/g at the surface to $19 \pm 0.39 \times 10^8$ atoms/g at 63 cm. Below 63 cm, $^{10}Be_m$ decreases, but increases once more with depth to $21 \pm 0.39 \times 10^8$ atoms/g at 99 cm depth. Concentrations of $^{10}Be_m$ at VF-1 show a general increase from $4.3 \pm 0.13 \times 10^8$ atoms/g at the surface to $20 \pm 0.35 \times 10^8$ atoms/g at a depth of 63 cm.

5.0 Discussion

The characteristic depth profiles of measured bulk OSL and $^{10}Be_m$ data through PSA deposits in Birchams Creek and at potential PSA sources allow us to assess the likelihood of different erosion histories for the creek in a way that would not be possible with one sediment tracing technique alone. While the measured bulk OSL and $^{10}Be_m$ data we present are specific to Birchams Creek, the combined fingerprinting technique and the interpretation we draw from the two datasets is adaptable elsewhere.

5.1 Reliability of bulk OSL and $^{10}Be_m$ data

The depth trends of bulk OSL data through PSA and SM sediments at Birchams Creek resemble SM and SM-PSA profiles found elsewhere in the Tablelands [*Muñoz-Salinas et al.*, 2014; *Portenga et al.*, 2016a] (Figure 5a); we note, however, that SM sediments at ~90 cm deep at site SM-1 show a substantial decrease in bulk OSL that is not observed in SM sediment profiles elsewhere in the Tablelands [*Portenga and Bishop*, 2016]. Without further sampling or deriving ages throughout the SM-1 profile, we can only speculate that this decrease may represent a former valley bottom surface. Bulk OSL data previously measured through profiles of weathered bedrock show relatively little luminescence in the uppermost horizons and in

increase of bulk OSL data with depth [*Muñoz-Salinas et al.*, 2014]. The bulk OSL depth trend at VF-1 is not similar to bulk OSL depth trends through weathered bedrock profiles, but instead appears to consist of up to three sequences of sediment deposited with inherited luminescence, suggested by the increases of bulk OSL in the profile at ~15 cm, ~50 cm, and ~80 cm. Floods deep enough to rise over the gully wall or fast enough to entrain and deposit the gravels present in the uppermost 6 cm at VF-1 are unlikely this far up an already small catchment. Thus, we suggest that the sediment exposed at VF-1 reflects sediment mobilized to the valley bottom by hillslope processes with some degree of inherited luminescence from the sediment's source.

Concentrations of $^{10}Be_m$ in soil depth profiles around the world are typically greatest in the near-surface and decrease with depth [*Graly et al.*, 2010; *Willenbring and von Blanckenburg*, 2010], though increases of $^{10}Be_m$ at depth have been observed in saprolite horizons of soil profiles in the nearby Burra Creek catchment [*Fifield et al.*, 2010]. Like $^{10}Be_m$ data from Burra Creek, the $^{10}Be_m$ increase we observe in the subsurface of the VF-1 profile is at depth; however, we suggest that the increase we observe in Birchams Creek is due to the greater proportion of fine grain sizes at depth at VF-1, which provide a greater surface area onto which $^{10}Be_m$ is adsorbed (Figure 3).

5.2 Identifying PSA source locations and depths

PSA deposits throughout the Tablelands were transported and deposited by floods; the higher bulk OSL measurements at the base of PSA compared to that in the uppermost SM sediments indicate that PSA was minimally bleached before deposition and that peak bulk OSL measurements reflect bulk OSL from the PSA source material [*Muñoz-Salinas et al.*, 2014; *Portenga and Bishop*, 2016; *Portenga et al.*, 2016a]. Thus, to be considered as a reasonable source for PSA, potential sources of PSA (e.g. SM-1, VF-1) must contain sediment with bulk OSL values greater than or equal to the bulk OSL maxima of PSA deposits (e.g. PSA-1, PSA-2; Figure 5a). Similarly, the initial incision depth of a gully is given by whatever depth is required to erode sediment with bulk OSL data greater than or equal to the bulk OSL maxima of PSA deposits (Figure 5a). Based on the similar and homogeneous inventories of $^{10}Be_m$ in PSA at PSA-1 and PSA-2 (~8.2×10^8 atoms/g), we suggest that potential PSA source locations and depths are determined by averaging the $^{10}Be_m$ inventories at SM-1 and VF-1 with depth until the average exceeds that of the PSA deposits (Figure 5b).

Based on our bulk OSL measurements, the DGECM is only a valid erosion model if SM-1 is incised to a depth between 39–89 cm and VF-1 is incised to a depth of 9–18 cm, thus providing sediment at PSA-1 and PSA-2, respectively, with sufficiently high levels of inherited luminescence (Figure 5, Table 3). VF-1 could be incised to a depth of 81 cm before it exceeds the average $^{10}Be_m$ concentration at PSA-2, but incising SM-1 to any depth greater than 12 cm results in $^{10}Be_m$ concentrations significantly greater than that observed at PSA-1. Thus, it follows that because shallow erosion of 9–18 cm at VF-1 adequately explains the $^{10}Be_m$ and bulk OSL data at PSA-2, it can be considered a source for PSA at PSA-2; however, because there is no overlap at SM-1 of the depths required to supply PSA-1 with both the measured $^{10}Be_m$ and bulk

OSL data, it is not a likely source. Our data therefore do not support the validity of the DGECM in explaining the erosion and PSA deposition history at Birchams Creek. Our data show that bulk OSL measured at PSA-1 could be derived from at least 15 cm of incision at VF-1 and that $^{10}Be_m$ measured at PSA-1 would not be exceeded unless VF-1 was eroded to a depth of >45 cm (Table 1); therefore, shallow incision of VF-1 (~15 cm) could also supply adequate amounts of inherited luminescence and $^{10}Be_m$ to PSA-1 as well as to PSA-2. We therefore conclude that the only plausible erosion scenario for Birchams Creek is the SSECM, in which only VF is incised, releasing sediment that is subsequently deposited downstream as PSA at multiple sites. This conclusion is supported by findings from other studies demonstrating how SM wetlands resist erosion [*Prosser and Slade*, 1994; *Zierholz et al*., 2001].

We further support our interpretation by showing that shallow incision (15 cm) at and upstream of VF-1 can provide the volume of PSA at PSA-1 and PSA-2 and balance the isotopic budget in the PSA deposits, considering that the valley-bottom ponds from 1880 CE are now also filled with PSA and the whole valley bottom is blanketed by PSA (Figure 1). The volume of the ponds in 1880 CE is 2,510 m^3, estimated from maps and pond surface area-depth relationships [*Eyles*, 1977a]. The remaining volume of PSA deposited across the valley bottom is estimated to be 290 m^3, which is the areal extent of areas with low slope (≤1°, using 30 m-resolution SRTM elevation data [*Jarvis et al.*, 2008]) and a depth of 21 cm at PSA-1 (indicated by the gravel horizon deposited over the filled ponds, Figure 3) and a depth of 63 cm at PSA-2. The total estimated volume of PSA in Birchams Creek is 2,800 m^3, and corresponds to a total $^{10}Be_m$ inventory of 3.2×10^{18} atoms, using the average PSA $^{10}Be_m$ isotopic concentration at PSA-1 and PSA-2. The sediment volume of the PSA deposits is matched by erosion ~15 cm deep and 11.9 m wide (average *b*-axis of ponds mapped in 1941 CE) along 3,190 m of the valley bottom at and upstream of VF-1; such erosion along the valley bottom upstream of VF-1 also supplied sufficient $^{10}Be_m$ to balance the $^{10}Be_m$ inventory measured from the PSA deposits. Eyles [1977a] shows that 3,730 m of the valley bottom was eroded by 1941 CE meaning that 86% of the sediment derived from initial incision along the eroded length of Birchams Creek is preserved on the landscape as PSA. This result agrees with previous findings showing that the majority of sediment eroded during gully incision in the Tablelands remains close to its source [*Melville and Erskine*, 1986].

5.3 Triggering mechanism for gully erosion at Birchams Creek

The timing of PSA deposition at Birchams Creek between 1914–1932 CE is provided both anecdotally and quantitatively [*Eyles*, 1977a; *Portenga et al.*, 2016b], and this study suggests where and how deep gullies first incised within the watershed. We have yet, however, to identify what triggered erosion in the first place. We explore the likelihood that the shear stress of stream flow associated with increased rainfall during otherwise arid conditions overcame the shear resistance of the valley bottom sediment at VF-1 to trigger gully incision [*Melville and Erskine*, 1986; *Patton and Schumm*, 1975; *Prosser and Abernethy*, 1996; *Prosser and Slade*, 1994]. The relationship between the critical slope threshold (S_{cr}, given as % gradient)

and upstream catchment area (A, in hectares) is provided by $S_{cr} = aA^{-b}$, where a and b are site specific constants that account for local climate and erodibility [*Vandaele et al.*, 1996]. With the exception of Birchams Creek, initial gully incision sites are largely unknown in the Tablelands; thus, S_{cr} and A of gullied creeks are unmeasurable, and a and b cannot be derived empirically. We therefore substitute a range of values, derived for valley-bottom gullies in Europe that have soil textures and mean annual rainfall similar to those at Birchams Creek (a = 0.025–0.09; b = -0.25– -0.4) [*Vandaele et al.*, 1996]. The upstream area of Birchams Creek at VF-1 is 306 ha, and the slope of the Birchams Creek valley bottom at VF-1 is ~1°, which requires $S_{cr} > 1.75$ for incision to occur. Using substituted values of a and b, S_{cr} in Birchams Creek ranges from 0.11–0.89 (or 4.7°–40°); thus, valley bottom slopes at VF-1, where the gully initially incised, would have to be ~5–40x steeper before incision could occur. Moreover, Eyles [1977a] observed that scour ponds in Birchams Creek are all found on valley bottom surfaces with the shallowest gradients – another indication that no topographic thresholds have been crossed. Thus, Birchams Creek is seemingly not steep enough to erode a gully; yet, erosion still occurred.

Vegetated catchments in the Tablelands have the capacity to withstand erosion from severe floods [*Neil and Fogarty*, 1991; *Zierholz et al.*, 2001]; therefore, if high rainfall triggered gully incision, severe vegetation degradation must have preceded gully initiation. In the early 1900s CE, the Tablelands was in the midst of a severe drought, as indicated by the near-total evaporation of endorheic Lake George [*Jacobson et al.*, 1991] (Figure 1). Furthermore, land use changed at this time from open eucalypt woodlands to cleared grazing pastures, which were used both by livestock and feral pigs [*Eyles*, 1977a]. In addition to overgrazing, the presence of livestock likely compacted soils, thereby decreasing soil infiltration and increasing the stream's ability to erode [*Trimble and Mendel*, 1995; *Warren et al.*, 1986]. Elsewhere in the Tablelands, congregating livestock created wallows, or depressions, in cleared valley bottoms that were observed to erode into deep gullies during breaks in severe droughts [*Eyles*, 1977b]. We therefore argue that livestock wallows in Birchams Creek created highly-localized oversteepened reaches ($\gg S_{cr}$) of the streambed at VF-1, which were then eroded by regionally high rainfall events that broke the drought in the early 1900s CE (see Figure 6 in Portenga et al. [2016b]). Such streamflow could reasonably initiate gully erosion and transport and deposit the PSA now observed in the lower Birchams Creek watershed.

The landscape history at Birchams Creek is similar to that documented for nearby Jerrabomberra Creek catchment [*Wasson et al.*, 1998]. Gully incision at both creeks illustrate the effects that European-introduced grazing practices likely had on erosion in the Tablelands, and we therefore suggest that the landscape history of Birchams Creek is representative of erosion histories of small headwater catchments throughout the Tablelands. We recognize, however, that while our explanation for the conditions leading to gully erosion is a plausible and reasonable erosion history for the relatively small Birchams Creek, it is uncertain whether larger catchments behaved similarly. That being said, our techniques and findings suggest that under the right circumstances, combined sediment tracing allows for reconstructions of gully incision, erosion,

and sediment deposition to be made, whether brought about by land-use changes or natural thresholds being crossed.

6.0 Conclusions

This study presents a novel dual sediment-fingerprinting technique that combines measurements of bulk OSL and $^{10}Be_m$ to identify, for the first time, the source location and source depth of gully-derived sediment. We demonstrate this technique in the southeastern Australian Tablelands – one of the most gully-affected landscapes in the world – by tracing PSA sediment deposited in Birchams Creek to its source location and estimating the depth from which is was eroded. In doing so, we test two conceptual models of gully development for the creek, and we confirm that all PSA in the catchment originated from shallow incision into valley fill in the creek's headwaters that eventually developed into gullies. This finding contrasts with the notion that gully development originated in reaches of the stream that were occupied by water-saturated swampy meadow wetlands. Sediment volumes, measurements of bulk OSL, and isotopic inventories of $^{10}Be_m$ between upstream erosional sources and downstream depositional locations are balanced, further supporting the notion that erosion of valley fill supplied downstream reaches of the creek with thick mantles of PSA. Our findings are consistent with conclusions drawn in nearby studies and with historical documentation. As this study incorporates a number of assumptions based on available historical documentation and findings from previous studies, the application of our techniques to assess gully erosion and PSA deposition in other landscapes around the world may be limited to locations where similar historical documentation is also available.

Acknowledgments and Data

This research was funded by a University of Glasgow International PhD Research Studentship and an International Macquarie University Research Excellence Scholarship. We thank the staff of the AMS Laboratory at SUERC for their support during beryllium isotopic analyses. The authors clarify that there are no conflicts of interest, perceived or otherwise, between funding sources or author affiliations and the outcome of this work. All data are presented in Tables S1 and S2 of the online Suppporting Information file. We thank Veronica Sosa-González, Lee Corbett, Tom Neilson, and Meredith Orr for field and laboratory assistance.

Tables

Table 1. Potential PSA source locations and depths

		DGECM		SSECM
		SM-1	VF-1	VF-1
PSA-1	Bulk OSL	39-89 cm 102-147 cm	---	~15 cm 69-99 cm
	^{10}Be $_{m}$	0-12 cm	---	0-45 cm
PSA-2	Bulk OSL	---	9-18 cm 63-99 cm	9-18 cm 63-99 cm
	^{10}Be $_{m}$	---	0-81 cm	0-81 cm

Figure Captions

Figure 1. The Birchams Creek watershed (BC, shaded white on inset figure) is a tributary of the Yass River, in the southeastern Australian Tablelands. C – Canberra, Australian Capital Territory; W – Wamboin, New South Wales. Main figure shows a time series illustrating gully development in Birchams Creek. The 1880 CE, 1941 CE, and 1975 CE time-steps are adapted from Eyles (1977a), and the 2013 CE time-step is drawn from satellite imagery and field site visits. Gully connectivity decreased during 1975–2013 CE as sediment became trapped behind farm dams (reservoirs) and sealed roads. Lower-case letters indicate locations where photographs shown in Figure 2 were taken.

Figure 2. Photographs of the field area. Photo locations are shown in Figure 1. (**a**) The contrast between totally and partially deforested hillslopes on the low-relief west hillslopes of Birchams Creek. Lower hillslopes grade into the valley bottom. Photograph taken facing south. (**b**) Modern gully with PSA and SM sediments exposed at site PSA-1. Gully walls are ~4 m in height. Photograph previously used in Portenga et al. [2016a], taken facing upstream. (**c**) Expansive modern gully eroding through SM sediments at SM-1. Gully walls are 1–3 m in height. SM-1 collected on south exposure. Photograph taken facing west. (**d**) Modern gully wall with PSA and SM sediments exposed at site PSA-2. Gully walls are ~3 m in height. Photograph taken facing downstream. (**e**) Valley fill sediments and distal hillslope deposits incised by the modern gully at VF-1. Sample profile extends to the bottom of the gully bed. Photograph taken facing west. (**f**) Swampy meadow wetlands and pond (in foreground) filling in the modern valley bottom above site VF-1. Ponds have migrated upstream since originally mapped in 1880 CE. Photograph taken facing north.

Figure 3. Photographic and textural descriptions sediment profiles for (**a**) PSA-1, (**b**) PSA-2, (**c**) SM-1, and (**d**) VF-1. Single-grain quartz OSL burial ages of post-European settlement alluvium and swampy meadow sediments at PSA-1 are from Portenga et al. [2016b]. Dashed white lines at

PSA-1 and PSA-2 indicate the bulk OSL transition depth from swampy meadow to post-European settlement alluvium sediment accumulation [Portenga et al., 2016a].

Figure 4. Schematic diagrams of profile locations and initial gully erosion models at Birchams Creek. (**a**) The discontinuous gully erosion model (DGECM) shows alluvium at PSA-1 originating in swampy meadow sediments at SM-1 (light blue coloring) and alluvium at PSA-2 originating in valley fill sediments at and upstream of VF-1 (dark blue coloring). (**b**) The single site erosion model (SSECM) shows alluvium at PSA-1 and PSA-2 originating in valley fill sediments at and upstream of VF-1 (orange coloring). Dotted black lines represent areas of erosion while solid black lines represent deposition. Continuous black line is Birchams Creek with black arrows indicating flow direction. Thin colored arrows indicate sediment transport and deposition direction.

Figure 5. Sediment transport pathways inferred from the DGECM. (**a**) Total bulk sediment OSL (black circles) at each profile site and the 3-sample average bulk OSL used for analyses in this study (black line). Uncertainties are many orders of magnitude less than the data points; thus, uncertainties are not shown, but can be found in Supplementary Table 1. Dashed black lines are at the SM-PSA transition, as interpreted from bulk OSL data and sediment texture descriptions. Solid light and dark blue boxes at PSA-1 and PSA-2, respectively, show the depths of peak inherited OSL. Dashed light and dark blue boxes at SM-1 and VF-1, respectively, indicate the depths where bulk OSL data are greater than or equal to bulk OSL maxima at PSA-1 and PSA-2, and thus represent the potential depths from which PSA at sites PSA-1 and PSA-2, respectively, could have originated under the DGECM. Bold arrows indicate pathways of sediment transportation from potential sources to PSA deposits. Note x-axis for SM-1 is not the same as the others. (**b**) Concentrations of $^{10}Be_m$ at each profile site (black circles). Uncertainties are many orders of magnitude less than the data points; thus, uncertainties are not shown, but can be found in Supplementary Table 2. Solid light and dark blue boxes at PSA-1 and PSA-2 indicate the depths over which $^{10}Be_m$ concentrations are averaged in PSA deposits. Dashed light and dark blue boxes at SM-1 and VF-1 indicate the respective source depths from which PSA at sites PSA-1 and PSA-2 could have originated under the DGECM. Bold arrows indicate pathways of sediment transport from potential sources to PSA deposits.

Figure 6. Sediment transport pathways inferred from the SSECM. (**a**) Total bulk sediment OSL (black circles) at each profile site and the 3-sample average bulk OSL used for analyses in this study (black line). Uncertainties are many orders of magnitude less than the data points; thus, uncertainties are not shown, but can be found in Supplementary Table 1. Dashed black lines are at the SM-PSA transition, as interpreted from bulk OSL data and sediment texture descriptions. Solid orange boxes at PSA-1 and PSA-2, respectively, show the depths of peak inherited OSL. Dashed orange box at VF-1 indicates the depths where bulk OSL data are greater than or equal to bulk OSL maxima at PSA-1 and PSA-2, and thus represent the potential depths from which PSA

at sites PSA-1 and PSA-2, respectively, could have originated under the SSECM. Bold arrows indicate pathways of sediment transportation from potential sources to PSA deposits. (**b**) Concentrations of $^{10}Be_m$ at each profile site (black circles). Uncertainties are many orders of magnitude less than the data points; thus, uncertainties are not shown, but can be found in Supplementary Table 2. Solid orange boxes at PSA-1 and PSA-2 indicate the depths over which $^{10}Be_m$ concentrations are averaged in PSA deposits. Dashed orange box at VF-1 indicates the source depths from which PSA at sites PSA-1 and PSA-2 could have originated under the DGECM. Bold arrows indicate pathways of sediment transport from potential sources to PSA deposits.

References

Aitken, M. J. (1998), *An Introduction to Optical Dating: The Dating of Quaternary Sediments by the Use of Photon-stimulated Luminescence*, 267 pp., Oxford University Press, Oxford, UK.

Beach, T., N. Dunning, S. Luzzadder-Beach, D. E. Cook, and J. Lohse (2006) Impacts of the ancient Maya on soils and soil erosion in the central Maya lowlands, *Catena*, *65*(2), 166–178, doi:10.1016/j.catena.2005.11.007.

Bierman, P. R., R. Coppersmith, K. Hanson, J. Neveling, E. W. Portenga, and D. H. Rood (2014) A cosmogenic view of erosion, relief generation, and the age of faulting in southern Africa, *GSA Today*, *24*(9), 4–11, doi:10.1130/GSATG206A.1.

Blisniuk, K., M. Oskin, K. Fletcher, T. Rockwell, and W. Sharp (2012) Assessing the reliability of U-series and ^{10}Be dating techniques on alluvial fans in the Anza Borrego Desert, California, *Quaternary Geochronology*, *13*, 26–41, doi: 10.1016/j.quageo.2012.08.004.

Bradley, N. D., and G. E. Tucker (2012), Measuring gravel transport and dispersion in a mountain river using passive radio tracers, *Earth Surface Processes and Landforms*, *37*(10), 1034–1045, doi:10.1002/esp.3223.

Brannstrom, C., and A. M. S. Oliveira (2000) Human modification of stream valleys in the western plateau of São Paulo, Brazil: implications for environmental narratives and management, *Land Degradation & Development*, *11*(6), 535–548, doi:10.1002/1099-145X(200011/12)11:6<535::AID-LDR412>3.0.CO;2-L.

Brown, L., M. J. Pavich, R. E. Hickman, J. Klein, and R. Middleton (1988), Erosion of the eastern United States observed with 10Be, *Earth Surface Processes and Landforms*, *13*(5), 441–457, doi:10.1002/esp.3290130509.

Coltorti, M., J. D. Fazie, F. P. Rios, and G. Tito (2010) The Ñuagapua alluvial fan sequence: Early and Late Holocene human-induced changes in the Bolivian Chaco? *Proceedings of the Geologists' Association*, *121*(2), 218–228, doi:10.1016/j.pgeola.2009.11.003.

Coronato, F. R. and H. F. del Valle (1993) Methodological comparison in the estimate of fluvial erosion in an arid closed basin of northeastern Patagonia, *Journal of Arid Environments*, *24*, 231–239, doi:10.1006/jare.1993.1021.

Cox, R., D. B. Zentner, A. F. M. Rakotondrazafy, and C. F. Rasoazanamparany (2010), Shakedown in Madagascar: Occurrence of lavakas (erosional gullies) associated with seismic activity, *Geology*, *38*(2), 179–182, doi:10.1130/G30670.1.

Crouch, R. J. (1987), The relationship of gully sidewall shape to sediment production, *Australian Journal of Soil Research*, *25*(4), 531–539.

Damm, B. and J. Hagedorn (2010) Holocene floodplain formation in the southern Cape region, South Africa, *Geomorphology*, *122*, 213–222, doi: 10.1016/j.geomorph.2009.06.025.

D'Haen, K., G. Verstraeten, and P. Degryse (2012) Fingerprinting historical fluvial sediment fluxes, *Progress in Physical Geography*, *36*(2), 154–186, doi:10.1177/0309133311432581.

diCenzo, P. D. and S. Luk (1997) Gully erosion and sediment transport in a small subtropical catchment, South China, *Catena*, *29*(2), 161–176, doi:10.1016/S0341-8162(96)00053-7.

Dosseto, A. and M. Schaller (2016) The erosion response to Quaternary climate change quantified using uranium isotopes and *in situ*-produced cosmogenic nuclides, *Earth-Science Reviews*, *115*, 60–81, doi: 10.1016/j.earscirev.2016.01.015.

Dosseto, A., S. P. Turner, and J. Chappell (2008) The evolution of weathering profiles through time: New insights from uranium-series isotopes, *Earth and Planetary Science Letters*, *274*(3–4), 359–371, doi: 10.1016/j.epsl.2008.07.050.

Dugmore, A. J., A. J. Newton, L. Guðrún, and G. T. Cook (2000) Tephrochronology, environmental change and the Norse settlement of Iceland, *Environmental Archaeology*, *5*(1), 21–34, doi:10.1179/env.2000.5.1.21.

Eriksson, M. G., J. M. Olley, D. R. Kilham, T. Pietsch, and R. J. Wasson (2006), Aggradation and incision since the very late Pleistocene in the Naas River, south-eastern Australia, *Geomorphology*, *81*(1–2), 66–88, doi:10.1016/j.geomorph.2006.04.001.

Eyles, R. J. (1977a), Birchams Creek: the transition from a chain of ponds to a gully, *Australian Geographical Studies*, *15*(2), 146–157, doi:10.1111/j.1467-8470.1977.tb00094.x.

Eyles, R. J. (1977b), Changes in drainage networks since 1820, Southern Tablelands, N.S.W, *Australian Geographer*, *13*(6), 377–386, doi:10.1080/00049187708702716.

Fifield, L. K., R. J. Wasson, B. Pillans, and J. O. H. Stone (2010), The longevity of hillslope soil in SE and NW Australia, *Catena*, *81*(1), 32–42, doi:10.1016/j.catena.2010.01.003.

Foulds, S. A., M. G. Macklin, and P. A. Brewer (2013) Agro-industrial alluvium in the Swale catchment, northern England, as an event marker for the Anthropocene, *The Holocene*, *0*(0), 1–16, doi: 10.1177/0959683612465445.

Fuchs, M., A. Lang, and G. A. Wagner (2004) The history of Holocene soil erosion in the Phlious Basin, NE Peloponnese, Greece, based on optical dating, *The Holocene*, *14*(3), 334–345, doi: 10.1191/0959683604hl710rp.

Gellis, A. C., M. J. Pavich, A. L. Ellwein, S. Aby, I. Clark, M. E. Wieczorek, and R. Viger (2011) Erosion, storage, and transport of sediment in two subbasins of the Rio Puerco, New Mexico, *Geological Society of America Bulletin*, *124*(5–6), 817–841, doi: 10.1130/B30392.1.

Graly, J. A., P. R. Bierman, L. J. Reusser, and M. J. Pavich (2010), Meteoric ^{10}Be in soil profiles - A global meta-analysis, *Geochimica et Cosmochimica Acta*, *74*(23), 6814–6829, doi:10.1016/j.gca.2010.08.036.

Helz, G. R., and N. Valette-Silver (1992), Beryllium-10 in Chesapeake Bay sediments: an indicator of sediment provenance, *Estuarine, Coastal and Shelf Science*, *34*(5), 459–469, doi:10.1016/S0272-7714(05)80117-9.

Hooke, R. L., J. F. Martín-Duque, and J. Pedraza (2012) Land transformation by humans: a review, *GSA Today*, *22*(12), 4–10, doi:10.1130/GSAT151A.1.

Jacobson, G., J. Jankowski, and R. S. Abell (1991), Groundwater and surface water interaction at Lake George, New South Wales, *BMR Journal of Australian Geology and Geophysics*, *12*, 161–190.

Jain, M., A. S. Murray, and L. Bøtter-Jensen (2004) Optically stimulated luminescence dating: How significant is incomplete light exposure in fluvial environments? *Quaternaire*, *15*, 143–157, doi:10.3406/quate.2004.1762.

Jarvis, A., H. I. Reuter, A. Nelson, and E. Guevara (2008) Hole-filled seamless SRTM data V$, International Centre for Tropical Agriculture (CIAT), available from http://srtm.csi.cgiar.org.

Kidder, T., L. Haiwang, Q. Xu, and M. Li (2012) The alluvial geoarchaeology of the Sanyangzhuang Site on the Yellow River floodplain, Hanan Province, China, *Geoarchaeology*, *27*(4), 324–343, doi:10.1002/gea.21411.

Knox, J. C. (2006), Floodplain sedimentation in the Upper Mississippi Valley: Natural versus human accelerated, *Geomorphology*, *79*, 286–310, doi:10.1016/j.geomorph.2006.06.031.

Krause, A. K., S. W. Franks, J. D. Kalma, R. J. Loughran, and J. S. Rowan (2003), Multi-parameter fingerprinting of sediment deposition in a small gullied catchment in SE Australia, *Catena*, *53*, 327–348, doi: 10.1016/S0341-8162(03)00083-7.

Lal, D., and B. Peters (1967), Cosmic ray produced radioactivity on the earth, in *Handbuch der Physik*, edited by K. Sitte, pp. 551–612, Springer-Verlag, New York.

Lamarre, H., B. MacVicar, and A. G. Roy (2005), Using Passive Integrated Transponder (PIT) Tags to Investigate Sediment Transport in Gravel-Bed Rivers, *Journal of Sedimentary Research*, *75*(4), 736–741, doi:10.2110/jsr.2005.059

Luk, S. H., Q. Y. Yao, J. Q. Gao, J. Q. Zhang, Y. G. He, and S. M. Huang (1997) Environmental analysis of soil erosion in Guangdong Province: A Deqing case study, *Catena*, *29*(2), 97–113, doi:10.1016/S0341-8162(96)00049-5.

Ma, L., J. Chabaux, N. West, E. Kirby, L. Jin, and S. Brantley (2013) Regolith production and transport in the Susquehanna Shale Hills Critical Zone Observatory, Part 1: Insights from U-series isotopes, *Journal of Geophysical Research: Earth Surface*, *118*(2), 722–740, doi: 10.1002/jgrf.20037.

Mactaggart, B., J. Bauer, D. Goldney, and A. Rawson (2008), Problems in naming and defining the swampy meadow: An Australian perspective, *Journal of Environmental Management*, *87*(3), 461–473, doi:10.1016/j.jenvman.2007.01.030.

Melville, M. D., and W. Erskine (1986), Sediment remobilization and storage by discontinuous gullying in humid southeastern Australia, in *Drainage Basin Sediment Delivery*, edited by R. F. Hadley, pp. 277–286, International Association of Hydrological Sciences.

Monaghan, M. C., S. Krishnaswami, and K. K. Turekian (1986), The global-average production rate of ^{10}Be, *Earth and Planetary Science Letters*, *76*(3–4), 279–287, doi:10.1016/0012-821X(86)90079-8.

Montgomery, D. R. (2007) *Dirt: The Erosion of Civilizations*, Berkeley, California, USA, University of California Press, 295 p.

Mould, S and K. Fryirs, 2017, The Holocene evolution and geomorphology of a chain of ponds, southeast Australia: Establishing a physical template for river management, *Catena*, *149*, 349–362, doi:10.1016/j.catena.2016.10.012.

Muñoz-Salinas, E., P. Bishop, D. C. W. Sanderson, and J.-J. Zamorano (2011) Interpreting luminescence data from a portable OSL reader: three case studies in fluvial settings, *Earth Surface Processes and Landforms*, *36*(*5*), 651–660, doi:10.1002/esp.2084.

Muñoz-Salinas, E., P. Bishop, D. Sanderson, and T. Kinnaird (2014), Using OSL to assess hypotheses related to the impacts of land-use change with the early nineteenth century arrival of Europeans in south-eastern Australia: An exploratory case study from Grabben Gullen Creek, New South Wales, *Earth Surface Processes and Landforms*, *39*(12), 1576–1586, doi:10.1002/esp.3542.

Neil, D., and P. Fogarty (1991), Land use and sediment yield on the southern Tablelands of New South Wales, *Australian Journal of Soil and Water Conservation*, *4*(2), 33–39.

Nelson, A. H., P. R. Bierman, J. D. Shakun, and D. H. Rood (2014), Using *in situ* cosmogenic ^{10}Be to identify the source of sediment leaving Greenland, *Earth Surface Processes and Landforms*, *39*, 1087–1100, doi:10.1002/esp.3565.

Nichols, K. K., P. R. Bierman, and D. H. Rood (2014), ^{10}Be constrains the sediment sources and sediment yield to the Great Barrier Reef from the tropical Barron River catchment, Queensland, Australia, *Geomorphology*, *224*, 102–110, doi:10.1016/j.geomorph.2014.07.019.

Nissen, E. K., J. R. P. Walker, A. Bayasgalan, A. Carter, M. Fattahi, E. Molor, C. Schnabel, A. J. West, and S. Xu (2009) The late Quaternary slip-rate of the Har-Us-Nuur fault (Mongolian Altai) from cosmogenic ^{10}Be and luminescence dating, *Earth and Planetary Science Letters*, *286*(3–4), 467–478, doi:10.1016/j.epsl.2009.06.048.

Nyssen, J., J. Poesen, J. Moeyersons, J. Deckers, M. Haile, and A. Lang (2004), Human impact on the environment in the Ethiopian and Eritrean highlands - a state of the art, *Earth-Science Reviews*, *64*, 273–320.

Olley, J., G. Caitcheon, and A. Murray (1998), The distribution of apparent dose as determined by Optically Stimulated Luminescence in small aliquots of fluvial quartz: Implications for dating young sediments, *Quaternary Geochronology*, *17*(11), 1033–1040, doi:10.1016/S0277-3791(97)00090-5.

Olley, J. M., A. S. Murray, D. H. Mackenzie, and K. Edwards (1993), Identifying sediment sources in a gullied catchment using natural and anthropogenic radioactivity, *Water Resources Research*, *29*(4), 1037–1043, doi:10.1029/92wr02710.

Olley, J. M., and R. J. Wasson (2003), Changes in the flux of sediment in the Upper Murrumbidgee catchment, Southeastern Australia, since European settlement, *Hydrological Processes*, *17*(16), 3307–3320, doi:10.1002/hyp.1388.

Patton, P. C., and S. A. Schumm (1975), Gully erosion, northwestern Colorado: A threshold phenomenon, *Geology*, *3*(2), 88–90, doi:10.1130/0091-7613(1975)3<88:GENCAT>2.0.CO;2.

Perroy, R. L., B. Bookhagen, G. P. Asner, and O. A. Chadwick (2010) Comparison of gully erosion estimates using airborne and ground-based LiDAR on Santa Cruz Island, California, *Geomorphology*, *118*(3–4), 288–300, doi:10.1016/j.geomorph.2010.01.009.

Poesen, J., J. Nachtergaele, G. Verstraeten, and C. Valentin (2003), Gully erosion and environmental change: importance and research needs, *Catena*, *50*, 91–133, doi:10.1016/S0341-8162(02)00143-1.

Pope, K. O. and T. H. van Andel (1984) Late Quaternary alluviation and soil formation in the southern ARgolid: Its history, causes and archaeological implications, *Journal of Archaeological Science*, *11*(4), 281–306, doi:10.1016/0305-4403(84)90012-8.

Portenga, E. W., and P. Bishop (2016), Confirming geomorphological interpretations based on portable OSL reader data, *Earth Surface Processes and Landforms*, *41*(3), 427–432, doi:10.1002/esp.3834.

Portenga, E. W., P. Bishop, D. B. Gore, and K. E. Westaway (2016a), Landscape preservation under post-European settlement alluvium in the south-eastern Australian tablelands, inferred from portable OSL reader data, *Earth Surface Processes and Landforms*, doi:10.1002/esp.3942.

Portenga, E. W., K. E. Westaway, and P. Bishop (2016b), Timing of post-European settlement alluvium deposition in SE Australia: A legacy of European land-use in the Goulburn Plains, *The Holocene*, doi:10.1177/0959683616640047

Prosser, I. P. (1990), Fire, humans, and denudation at Wangrah Creek, southern Tablelands, N.S.W., *Australian Geographical Studies*, *28*(1), 77–95, doi:10.1111/j.1467-8470.1990.tb00623.x.

Prosser, I. P. (1991), A comparison of past and present episodes of gully erosion at Wangrah Creek, southern Tablelands, New South Wales, *Australian Geographical Studies*, *29*(1), 139–154, doi:10.1111/j.1467-8470.1991.tb00711.x.

Prosser, I. P., and B. Abernethy (1996), Predicting the topographic limits to a gully network using a digital terrain model and process thresholds, *Water Resources Research*, *32*(7), 2289–2298.

Prosser, I. P., and C. J. Slade (1994), Gully formation and the role of valley-floor vegetation, southeastern Australia, *Geology*, *22*(12), 1127–1130, doi:10.1130/0091-7613(1994)022<1127:gfatro>2.3.co;2.

Prosser, I. P., and S. J. Winchester (1996), History and processes of gully initiation and development in eastern Australia, *Zeitschrift für Geomorphologie, Supplementband 105*, 91–109.

Rengers, F. K., G. E. Tucker, J. A. Moody, and B. A. Ebel (2016), Illuminating wildfire erosion and deposition patterns with repeat terrestrial lidar, *Journal of Geophysical Research: Earth Surface*, *121*(3), 588–608, doi:10.1002/2015JF003600.

Reusser, L. J., and P. R. Bierman (2010), Using meteoric ^{10}Be to track fluvial sand through the Waipaoa River basin, New Zealand, *Geology*, *38*(1), 47–50, doi:10.1130/g30395.1.

Rhodes, E. J. (2007) Quartz single grain OSL sensitivity distributions: implications for multiple grain single aliquot dating, *Geochronometria*, *26*, 19–29, doi:10.2478/v10003-007-0002-5.

Richardson, J. M., I. C. Fuller, K. A. Holt, N. J. Litchfield, and M. G. Macklin (2014) Rapid post-settlement floodplain accumulation in Northland, New Zealand, *Catena*, *113*, 292–305, doi:10.1016/j.catena.2013.08.013.

Rittenour, T. M. (2008) Luminescence dating of fluvial deposits; applications to geomorphic, palaeoseismic and archaeological research, *Boreas*, *37*, 613–635, doi:10.1111/j.1502-3885.2008.00056.x.

Rosen, A. M. (2008) The impact of environmental change and human land use on the alluvial valleys in the Loess Plateau of China during the Middle Holocene, *Geomorphology*, *101*(1–2), 298–307, doi:10.1016/j.geomorph.2008.05.017.

Rustomji, P., and T. Pietsch (2007), Alluvial sedimentation rates from southeastern Australia indicate post-European settlement landscape recovery, *Geomorphology*, *90*(1–2), 73–90, doi:10.1016/j.geomorph.2007.01.009.

Sanderson, D. C. W., and S. Murphy (2010), Using simple portable OSL measurements and laboratory characterisation to help understand complex and heterogeneous sediment sequences for luminescence dating, *Quaternary Geochronology*, *5*(2-3), 299–305, doi:10.1016/j.quageo.2009.02.001.

Scott, A. (2001), Water erosion in the Murray-Darling Basin: Learning from the past, *Technical Report Rep. 43/01*, 134 pp, CSIRO Land & Water.

Stankovansky, M. (2003), Historical evolution of permanent gullies in the Myjava Hill Land, Slovakia, *Catena*, *51*, 223–239, doi:10.1016/S0341-8162(02)00167-4.

Starr, B. (1989), Anecdotal and relic evidence of the history of gully erosion and sediment movement in the Michelago Creek catchment area, NSW, *Australian Journal of Soil and Water Conservation*, *2*(3), 26–31.

Stock, G. M., P. A. Ehlers, and K. A. Farley (2006), Where does sediment come from? Quantifying catchment erosion with detrital apatite (U-Th)/He thermochronometry, *Geology*, *34*(9), 725–728, doi:10.1130/G22592.1.

Stone, J. (1998), A rapid fusion method for separation of beryllium-10 from soils and silicates, *Geochimica et Cosmochimica Acta*, *62*(3), 555–561.

Toy, T. J. (1982) Accelerated erosion: process, problems, and prognosis, *Geology*, *10*, 524–529, doi: 10.1130/0091-7613(1982)10<524:AEPPAP>2.0.CO;2.

Trimble, S. W., and A. C. Mendel (1995), The cow as a geomorphic agent – A critical review, *Geomorphology*, *13*, 233–253.

Turkelboom, F., J. Poesen, and G. Trébuil (2008) The multiple land degradation effects caused by land-use intensification in tropical steeplands: A catchment study from northern Thailand, *Catena*, *75*, 102–116, doi:10.1016/j.catena.2008.04.012.

Valette-Silver, J. N., L. Brown, M. Pavich, J. Klein, and R. Middleton (1986) Detection of erosion events using ^{10}Be profiles: Example of the impact of agriculture on soil erosion in the Chesapeake Bay area (U.S.A.), *Earth and Planetary Science Letters*, *80*(1–2), 82–90, doi:10.1016/0012-821X(86)90021-X.

Vandaele, K., J. Poesen, G. Govers, and B. van Wesemael (1996), Geomorphic threshold conditions for ephemeral gully incision, *Geomorphology*, *16*, 161–173, doi:10.1016/0169-555X(95)00141-Q.

Wallinga, J. (2002) Optically stimulated luminescence dating of fluvial deposits: a review, *Boreas*, *31*, 303–322, doi:10.1111/j.1502-3885.2002.tb01076.x.

Warren, S. D., T. L. Thurow, W. H. Blackburn, and N. E. Garza (1986), The influence of livestock trampling under intensive rotation grazing on soil hydrologic characteristics, *Journal of Range Management*, *39*(6), 491–495.

Wasson, R. J., G. Caitcheon, A. S. Murray, M. McCullogh, and J. Quade (2002) Sourcing sediment using multiple tracers in the catchment of Lake Argyle, northwestern Australia, *Environmental Management*, *29*(5), 634–646, doi:10.1007/s00267-001-0049-4.

Wasson, R. J., R. K. Mazari, B. Starr, and G. Clifton (1998), The recent history of erosion and sedimentation on the Southern Tablelands of southeastern Australia: sediment flux dominated by channel incision, *Geomorphology*, *24*(4), 291–308, doi:10.1016/S0169-555X(98)00019-1.

West, N., E. Kirby, P. Bierman, R. Slingerland, L. Ma, D. Rood, and S. Brantley (2013) Regolith production and transport in the Susuquehanna Shale Hills Critical Zone Observatory, Part 2: Insights from meteoric ^{10}Be, *Journal of Geophysical Research: Earth Surface*, *118*(3), 1877–1890, doi: 10.1002/jgrf.20121.

Wilkinson, M. T., and G. S. Humphreys (2005), Exploring pedogenesis via nuclide-based soil production rates and OSL-based bioturbation rates, *Australian Journal of Soil Research*, *43*(6), 767–779, doi:10.1071/SR04158.

Wilkinson, B. H. and B. J. McElroy (2007) The impact of humans on continental erosion and sedimentation, *Geological Society of America Bulletin*, *119*(1–2), 140–156, doi:10.1130/B25899.1.

Willenbring, J. K., and F. von Blanckenburg (2010), Meteoric cosmogenic Beryllium-10 adsorbed to river sediment and soil: Applications for Earth-surface dynamics, *Earth-Science Reviews*, *98*(1–2), 105–122.

Xu, S., S. P. H. T. Freeman, D. H. Rood, and R. M. Shanks (2015) Decadal ^{10}Be, ^{26}Al and ^{36}Cl QA measurements on the SUERC accelerator mass spectrometer, *Nuclear Instruments and Methods B: Beam Interactions with Materials and Atoms*, *361*, 39–42, doi:10.1016/j.nimb.2015.03.064.

Zierholz, C., J. P. Prosser, P. J. Fogarty, and P. Rustomji (2001), In-stream wetlands and their significance for channel filling and the catchment sediment budget, Jugiong Creek, New South Wales, *Geomorphology*, *38*(3–4), 221–235.

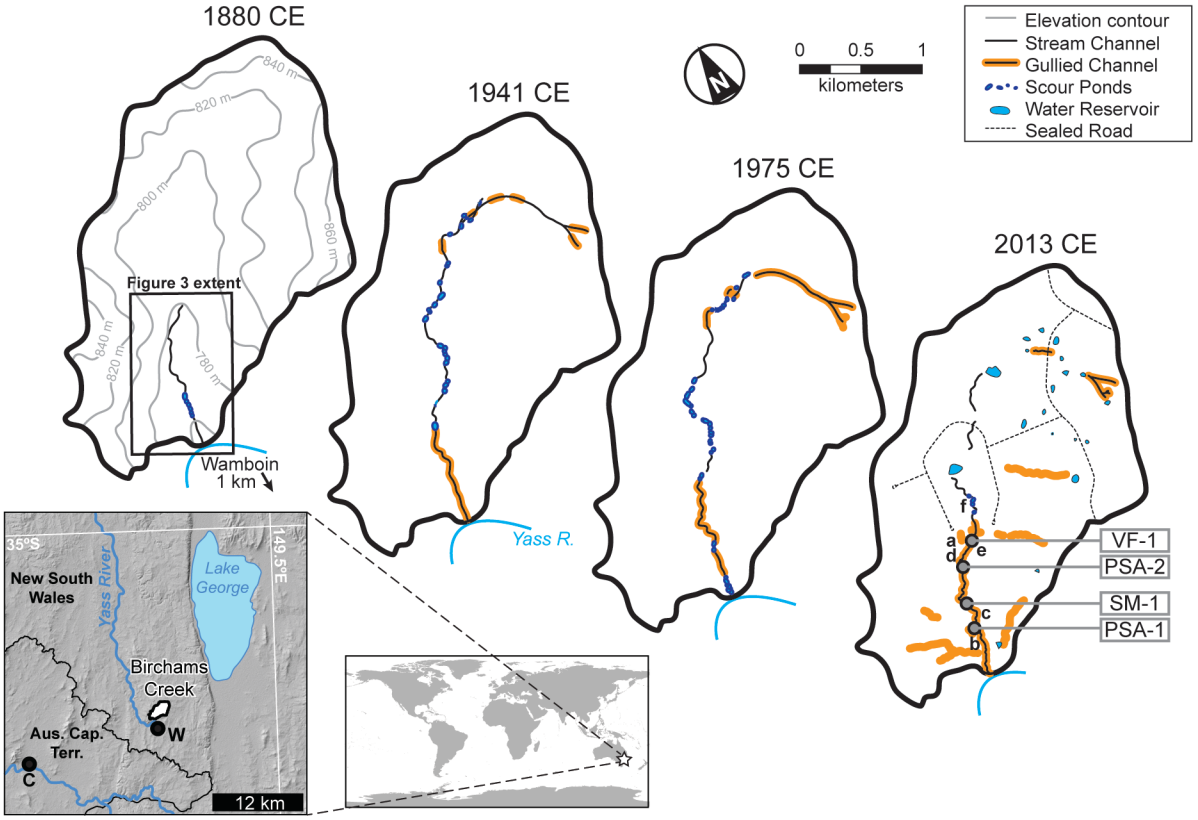

2016JF004052-f01-z-.tif

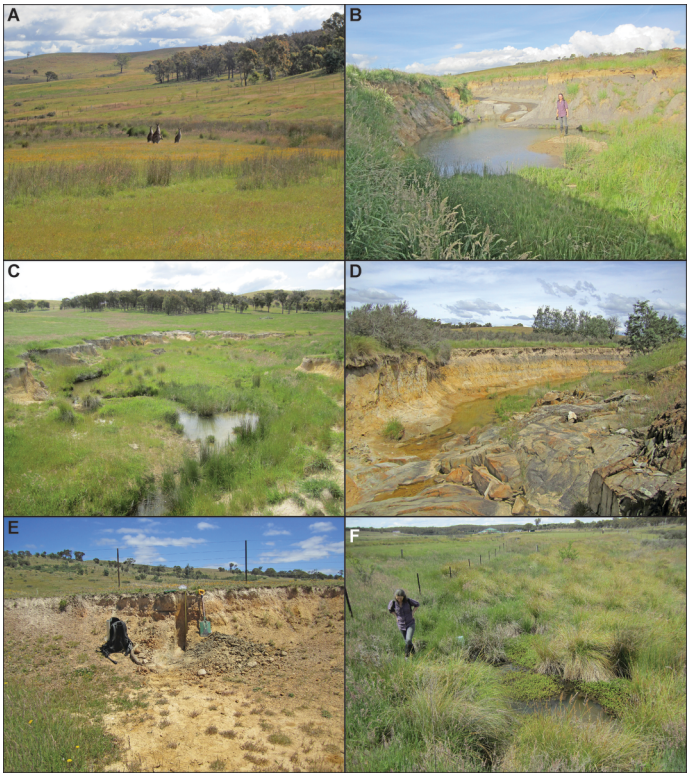

2016JF004052-f02-z-.tif

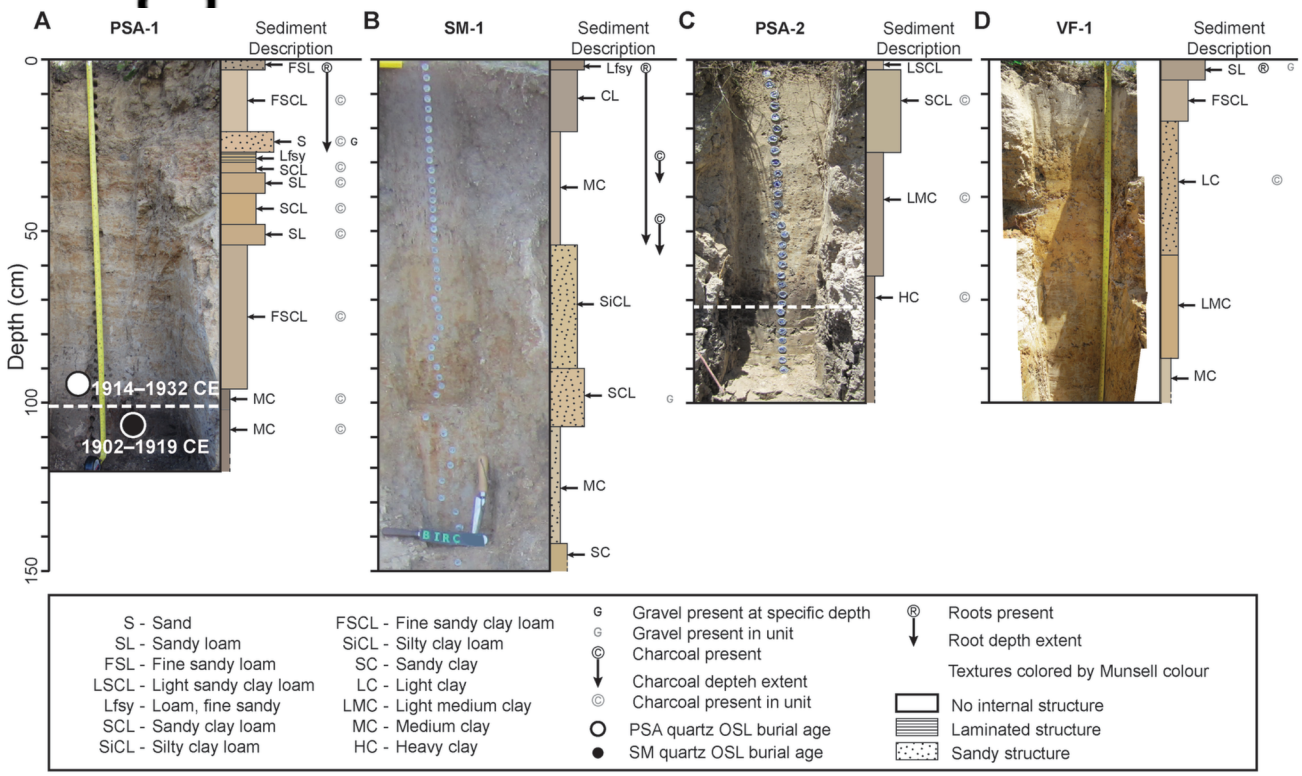

2016JF004052-f03-z-.tif

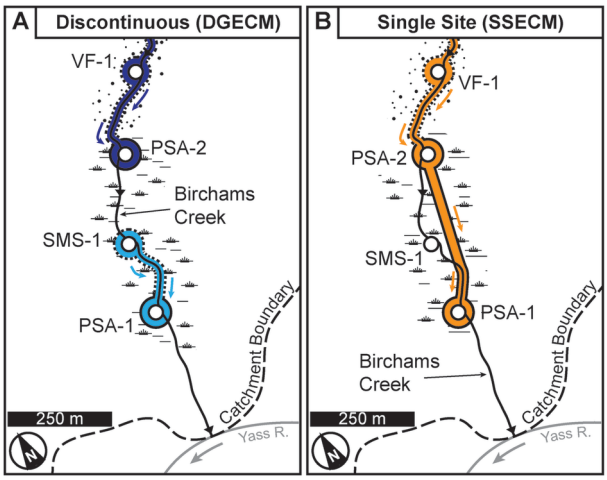

2016JF004052-f04-z-.tif

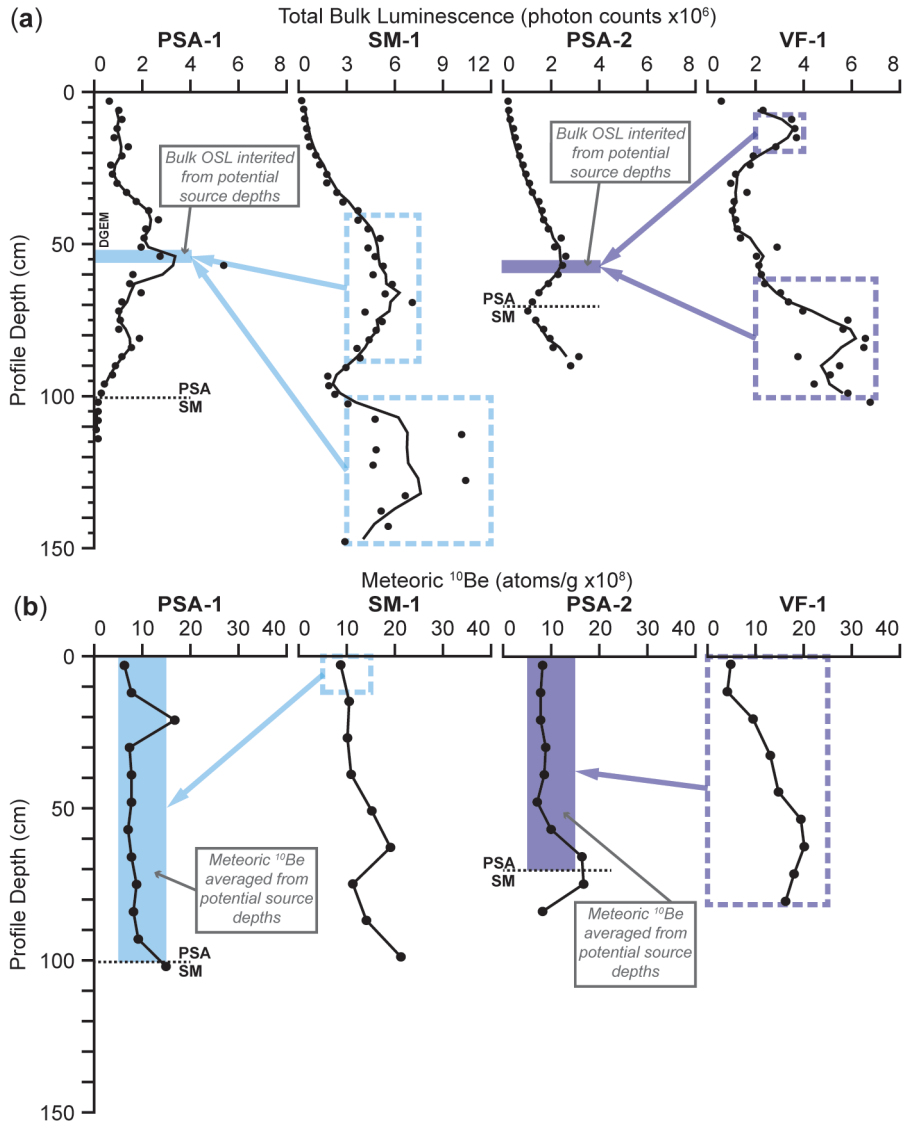

2016JF004052-f05-z-.tif

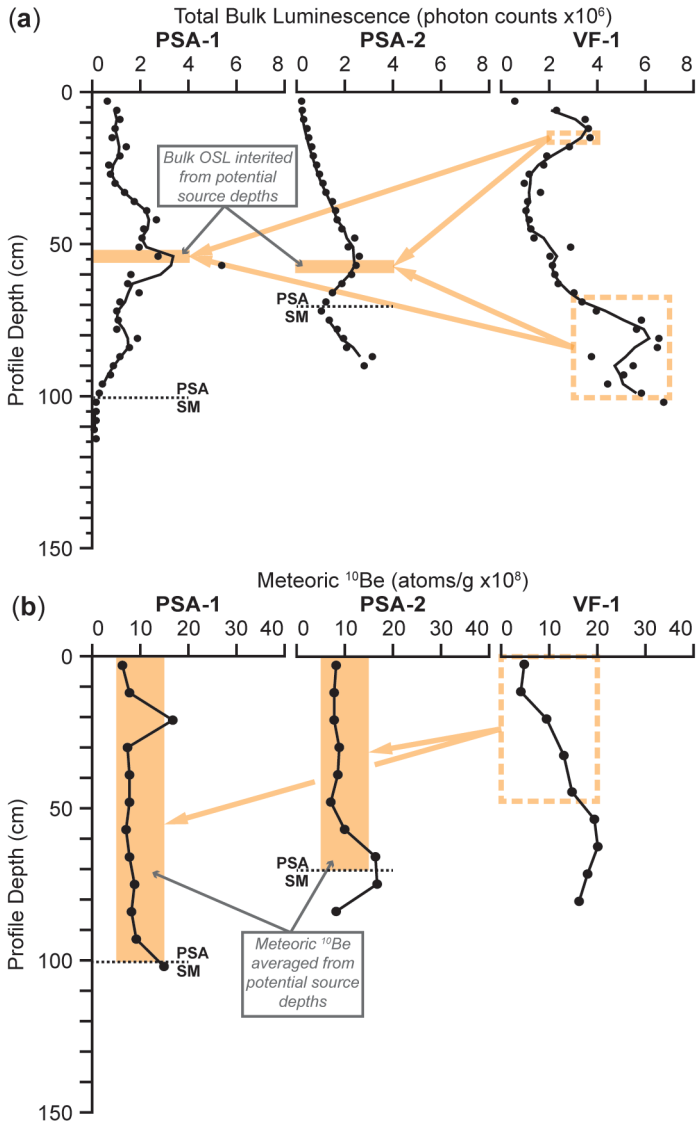

2016JF004052-f06-z-.tif